

**On the nature of active sites for formic acid decomposition  
on Au catalysts**

Journal:	<i>Catalysis Science &amp; Technology</i>
Manuscript ID	CY-ART-02-2019-000410.R1
Article Type:	Paper
Date Submitted by the Author:	18-Apr-2019
Complete List of Authors:	Li, Sha; University of Wisconsin-Madison, Chemical Engineering Singh, Suyash; University of Wisconsin System, Dumesic, James; University of Wisconsin, Chemical and Biological Engineering Mavrikakis, Manos ; University fo Wisconsin - Madison,

# On the nature of active sites for formic acid decomposition on Au catalysts

Received 00th January 20xx,  
Accepted 00th January 20xx

Sha Li<sup>a</sup>, Suyash Singh<sup>a</sup>, James A. Dumesic<sup>a</sup>, and Manos Mavrikakis<sup>a\*</sup>

DOI: 10.1039/x0xx00000x

Formic acid decomposition has been studied experimentally on supported gold nanoparticles with strong evidence showing the critical role of gold clusters in the subnanometer range in catalyzing the reaction. However, there is a lack of theoretical studies capable of explaining these experimental observations. In this work, without accounting for support effects, vapor phase formic acid decomposition was studied systematically on sub-nanometric gold clusters from Au<sub>4</sub> to Au<sub>25</sub>, among which several candidate Au clusters were identified as a promising active site model for the Au/SiC catalysts. Combining theoretical and experimental results suggested that the active site on Au/SiC catalysts could be represented by an Au<sub>18</sub> cluster, on which the reaction rates calculated from the microkinetic model closely match the experimentally measured rates. On Au<sub>18</sub>, formic acid decomposition proceeds through the same formate mediated pathway as that on extended Au surfaces ( $\text{HCOOH} \rightarrow \text{HCOO} + \text{H} \rightarrow \text{CO}_2 + 2\text{H} \rightarrow \text{CO}_2 + \text{H}_2$ ), with the reaction taking place on a triangular Au<sub>3</sub> site where the reactive Au atoms have a coordination number of 5. Despite the fact that other Au clusters among those studied, including Au<sub>17</sub> and Au<sub>19</sub> which also expose the same triangular Au<sub>3</sub> site, they were not found to be an accurate representation of the active sites, suggesting an atom-specific activity of gold clusters for formic acid decomposition.

## Introduction

Since the pioneering work of Haruta<sup>1, 2</sup> in the late 1980s showing that nanosized gold particles are effective catalysts for CO oxidation, gold nanoparticles (NPs) have attracted wide interest in the catalysis community<sup>3-7</sup>. Various catalytic reactions including CO oxidation<sup>8-22</sup>, propylene oxidation<sup>5, 17, 19, 23-25</sup>, water gas shift (WGS) reaction<sup>5, 17, 26-32</sup>, hydrogenation of unsaturated hydrocarbons<sup>17, 33-35</sup>, and hydrogen production from formic acid (HCOOH)<sup>36-41</sup> have been studied on supported gold NPs. In some cases, gold NPs show unique catalytic properties with unprecedented superior activities, allowing reactions to take place at significantly lower temperatures<sup>11, 19, 27, 28, 42, 43</sup> and to show high selectivity towards the desired products<sup>26, 37, 44</sup>. Among these reactions, formic acid decomposition provides an attractive route for utilizing large quantities of byproduct formic acid produced in biomass upgrading towards fuels and chemicals. The selective *in situ* generation of hydrogen, which is needed for biofuel upgrading, is the desired HCOOH decomposition reaction.<sup>45-47</sup> The first study of supported Au as an active catalyst for HCOOH decomposition was reported by Iglesia and colleagues<sup>37</sup>; they showed that well-dispersed Au species decompose HCOOH to H<sub>2</sub> and CO<sub>2</sub> exclusively, and exhibit turnover rates higher than supported Pt catalysts, one of the most active catalysts for HCOOH decomposition<sup>40, 41, 48, 49</sup>. Subsequent studies of this reaction by Ross<sup>39</sup> and Solymosi<sup>38</sup> over Au NPs supported on various supports, however, showed CO formation on most of the catalysts studied, and a promotion effect of added water was reported. Their observations may imply the occurrence of the WGS reaction

during HCOOH decomposition. This variance in selectivity of this reaction could be attributed to several different factors including catalyst preparation methods, gold particle size, reaction conditions and nature of the support.

Au catalysts used in the above-mentioned studies have a broad size distribution with an average particle size ranging from 2nm to 10nm. Adopting a modified deposition-precipitation procedure, Fan and coworkers<sup>44</sup> prepared Au/ZrO<sub>2</sub> catalysts with smaller sizes of less than 2nm and reported the highest turnover rate and lowest apparent activation energy (E<sub>a</sub>) for CO-free H<sub>2</sub> production from HCOOH. Based on their kinetic isotope effect studies, they proposed a reaction mechanism comprised of two sequential dehydrogenation steps of HCOOH through the formate (HCOO) intermediate and adsorbed atomic hydrogen recombination, which is consistent with one of the two mechanisms considered by Iglesia and colleagues<sup>37</sup>. The Au particle size in Au/ZrO<sub>2</sub> was estimated to be ca. 0.8nm based on CO titration measurement of the fresh and used catalysts, hinting the possibly critical role of subnanometric Au clusters in facilitating this reaction. Iglesia and colleagues<sup>37</sup> also suggested that the reactivity arises from highly dispersed Au species undetectable by microscopes. Flytzani-Stephanopoulos and coworkers<sup>36</sup> suggested that the active site for this reaction over Au/CeO<sub>2</sub> catalysts might be atomically dispersed species.

Despite the general consensus that smaller Au nanoparticles are crucial to achieve a high reactivity for HCOOH decomposition, the exact nature of the active sites in supported Au catalysts remains to be elucidated. In our previous work<sup>50</sup>, using a combination of density functional theory (DFT) calculations, experiments and microkinetic modeling, we concluded that HCOOH decomposition proceeds through the formate intermediate, followed by its decomposition and recombinative desorption of H<sub>2</sub>. However, the extended model surfaces of gold: (111), (100) and (211) with surface atoms coordination number (CN) of 9, 8, and 7,

<sup>a</sup> Department of Chemical and Biological Engineering, University of Wisconsin - Madison, Madison, WI, USA 53706

<sup>b</sup> \*corresponding author: Manos Mavrikakis; email: [emavrikakis@wisc.edu](mailto:emavrikakis@wisc.edu); phone: (608)262-9053; fax: (608)262-9053

respectively, were not capable of reproducing experimental data measured over the Au/SiC catalysts used in the experiments. Additional experiments conducted on different catalyst samples with a varying degree of dispersion in conjunction with relations determining the fraction of different types of Au sites as a function of average particle size suggested that coordinatively unsaturated corner sites are most likely the active sites responsible for measured reactivity. However, in that study, the physical models of Au clusters used to develop the relations between site density and particle size were truncated cuboctahedra, which may not represent the most stable structure of Au clusters, especially for the catalytically important sub nanometric Au clusters.

In this work, without considering support effects, the most stable configurations of sub nanometer Au clusters (up to a 25-atom cluster with a size of 0.85 nm) were investigated using *ab initio* molecular dynamics (AIMD) calculations. In addition, energetics of the elementary reactions for HCOOH decomposition were performed using DFT on several optimized Au clusters, most promising candidates for representing the active sites. We then combined these results with experiments and microkinetic analysis to arrive at the conclusion that, among all Au clusters studied, Au<sub>18</sub> appears to be the most likely one for representing the active site found in the Au/SiC catalysts used in our experiments. Importantly, Au<sub>18</sub> possess a triangular Au<sub>3</sub> site with CN=5 where the reaction most likely takes place.

## Results and Discussion

We will first discuss the minimum energy configurations of sub nanometric Au clusters (up to Au<sub>25</sub>), their binding properties for the key reaction intermediates, and the first dehydrogenation step in HCOOH decomposition on these clusters; analysis on the obtained results allows us to narrow down the candidate active site models to several Au clusters that are most promising. A reaction network comprised of 11 elementary steps is then evaluated on these promising Au clusters and the DFT calculated energetics are used to parameterize a microkinetic model. Comparison of the model predictions with the experimental results enables further down-selection of the active site models responsible for Au catalysis in HCOOH decomposition.

### Optimized Au<sub>n</sub> (n=2-25) clusters

Since the discovery of the extraordinary catalytic activity of highly dispersed gold nanoparticles toward CO oxidation by Haruta *et al.*<sup>1</sup>, considerable efforts have been devoted to understand the unique catalytic properties of gold. In particular, the detailed structure of small gold clusters, containing 3-20 gold atoms has been studied through a combination of theory and experiments<sup>51-66</sup>. However, most of these studies focused on charged Au clusters, anionic Au clusters because charged clusters are more easily size-selected. In addition, experimental techniques widely used to understand the geometric properties of Au clusters, including

ion mobility spectrometry, photoelectron spectroscopy, and trapped ion electron diffraction, are all restricted to charged species.<sup>67</sup> Compared to charged Au clusters, there is a lack of both experimental and theoretical studies for neutral Au clusters.

In this work, *ab initio* molecular dynamics simulations were used to obtain the most stable configurations of Au<sub>n</sub> (with n=2-25) clusters, which are shown in **Figure 1**. We find that 2-dimensional (2D) structures are preferred from Au<sub>2</sub> to Au<sub>16</sub>, while Au<sub>n</sub> clusters with more than 16 atoms prefer 3D structures. Most planar structures can be obtained from truncation of a monolayer (ML) of the Au(111) surface with the exception of Au<sub>8</sub>, which adopts a highly symmetric (*D*<sub>4h</sub> symmetry) star-shaped planar structure and represents a distinct type of site, where two squares are formed by the innermost and outermost four atoms with an angle of 45 degrees between their diagonals. Among the planar structures, Au<sub>6</sub> also has a highly symmetric structure (*D*<sub>3h</sub> symmetry), yielding an equilateral triangle. Au<sub>20</sub> is a tetrahedral pyramid with *T*<sub>d</sub> symmetry, a structure that has also been suggested to be the global minimum for anionic Au<sub>20</sub><sup>63</sup>. Removal of one, two and three corner atoms from the Au<sub>20</sub> tetrahedron leads to a truncated pyramid Au<sub>19</sub> with *C*<sub>3v</sub> symmetry, Au<sub>18</sub> with *C*<sub>2v</sub> symmetry, and Au<sub>17</sub> also with *C*<sub>3v</sub> symmetry, respectively. Addition of one, two and three atoms to Au<sub>20</sub> forms Au<sub>21</sub>, Au<sub>22</sub> and Au<sub>23</sub> which are pyramid structures with reduced symmetries. Au<sub>24</sub> is characterized by a highly asymmetric structure, while Au<sub>25</sub> can be formed by adding a layer of Au<sub>6</sub> triangular structure underneath the bottom layer of Au<sub>19</sub>. Among these 2D and 3D structures, the rhombic (*D*<sub>2h</sub>) Au<sub>4</sub>, trapezoid (*C*<sub>2v</sub>) Au<sub>5</sub>, edge-capped triangle (*C*<sub>s</sub>) Au<sub>7</sub>, four-fold edge-capped square Au<sub>8</sub>, truncated pyramid Au<sub>19</sub> and pyramid Au<sub>20</sub> have been confirmed by Fielicke and coworkers<sup>51, 60</sup> using far-infrared multiple-photon dissociation (FIR-MPD) spectroscopy, the only size-selective experimental technique available for structure determination of neutral metal clusters in the gas phase. While the 2D-to-3D transition has been found to appear in the range of n = 12-13 for gold cluster anions Au<sub>n</sub><sup>-</sup><sup>57, 58</sup>, it is yet to be determined experimentally for neutral Au clusters.

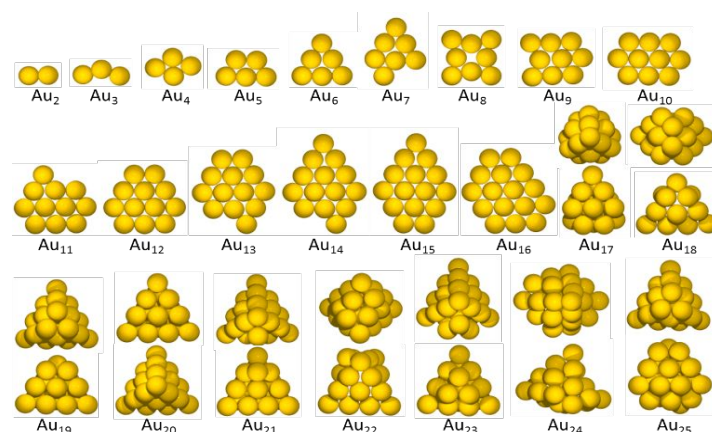


Figure 1 The most stable configurations of Au<sub>n</sub> (n=2-25) clusters obtained from AIMD simulations. Two views are provided for Au<sub>n</sub> clusters with 3D structures.

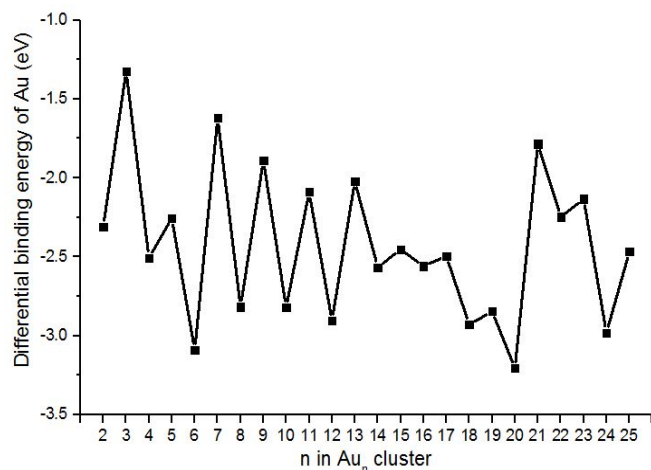


Figure 2 Differential binding energy (dBE) of Au in Au<sub>n</sub> (n=2-25) clusters using isolated atomic Au atom as the energy reference.  $dBE = E(Au_n) - E(Au_{n-1}) - E(Au)$ .

The differential binding energy (dBE) of Au in Au<sub>n</sub> clusters is calculated as the energy gained by adding the last Au atom to make a specific Au<sub>n</sub> cluster and is plotted in **Figure 2**. A pronounced odd-even oscillation appears in the differential binding energy of Au in these clusters, with even-numbered Au clusters being more stable than neighboring odd-numbered clusters, which can be understood by the effect of electron pairing in orbitals<sup>66, 68, 69</sup>. This phenomenon is part of the widely observed odd-even effects seen in properties such as electron affinities, ionization potentials, dissociation energies *etc.*<sup>70</sup> for coinage metal clusters<sup>71-77</sup> as well as monovalent alkali clusters<sup>71, 78-80</sup>. Based on the differential binding energy plot, Au<sub>6</sub> and Au<sub>20</sub> represent two of the most stable clusters among Au<sub>n</sub> clusters with no more than 25 atoms. Using energy of an Au atom in the bulk as reference (-3.20 eV), Au<sub>6</sub> and Au<sub>20</sub> are the only two clusters with negative dBE values, -0.06 eV for Au<sub>6</sub> and -0.18 eV for Au<sub>20</sub>, indicating that the last Au atom in these two clusters binds even more strongly than Au atoms to bulk Au. This enhanced stability of Au<sub>6</sub> and Au<sub>20</sub> results from their compact symmetric structures and fully filled electronic shells.<sup>81, 82</sup> Differential binding energy plot using bulk Au as the energy reference can be found in Supporting Information (SI; **Figure S1**).

#### Binding of key intermediates in HCOOH decomposition on Au<sub>n</sub> (n=4-25) clusters

After the structures of Au<sub>n</sub> clusters were optimized, binding energies of key intermediates in HCOOH decomposition, including HCOOH, formate (HCOO), carboxyl (COOH) and H were calculated on Au<sub>n</sub> (n=4-25) clusters. The most stable configurations of these four intermediates adsorbed on Au<sub>n</sub> clusters can be found in SI together with their respective binding energy (BE) values (**Figure S2**; **Table S1**). **Figure 3** compares the BE values on Au<sub>n</sub> clusters to those we obtained earlier on the Au(211) surface.

All Au<sub>n</sub> clusters bind HCOOH more strongly than Au(211) by ca. 0.15-0.50 eV, except for Au<sub>4</sub>, where HCOOH binds much more strongly (-1.02 eV) compared to -0.27 eV on Au(211). Binding strength of the closed-shell HCOOH species is less sensitive to the atomicity of gold clusters compared with the other three intermediates, of which the BEs also show an obvious odd-even oscillation, similar to that found for the dBE of Au in Au<sub>n</sub> clusters. As H, COOH, and HCOO all have an odd number of valence electrons, they bind more strongly to the odd-numbered Au<sub>n</sub> clusters than to their neighboring even-numbered clusters. Atomic H, in particular, binds more strongly to all the odd-numbered Au<sub>n</sub> (n=4-25) clusters than it does to Au(211), whereas the even-numbered clusters bind H similarly to Au(211) except for Au<sub>6</sub>, Au<sub>8</sub> and Au<sub>20</sub>, which bind H 0.3-0.5 eV weaker than Au(211). Compared with the Au(211) surface, binding strength of HCOO is stronger on all Au<sub>n</sub> (n=4-25) clusters except for Au<sub>6</sub>, Au<sub>8</sub> and Au<sub>20</sub>, where a 0.2-0.4 eV smaller BE of HCOO is determined. Similarly, all Au<sub>n</sub> (n=4-25) clusters bind COOH with a stronger strength than Au(211) except for Au<sub>6</sub> and Au<sub>20</sub>, on which a 0.1-0.2 eV weaker binding strength is observed for COOH. In general, Au<sub>6</sub>, Au<sub>8</sub> and Au<sub>20</sub> are found to have a weaker interaction with the probed intermediates, in accord with their relatively high stability and the completely filled electronic shells in their compact symmetric structures.

Being isomers of each other, the relative stability of HCOO and COOH was compared on each Au<sub>n</sub> (n=4-25) cluster with the energy difference being summarized in **Table 1**. We find that HCOO is more stable than COOH on all Au<sub>n</sub> (n=4-25) clusters except for Au<sub>6</sub>, where HCOO is slightly less stable than COOH by 0.02 eV. Compared against COOH, HCOO is stabilized to a higher extent on Au<sub>5</sub>, Au<sub>18</sub>, Au<sub>19</sub> and Au<sub>24</sub> than on Au(211), while this stabilization extent for HCOO is observed to be similar or smaller on the remaining clusters being investigated than on Au(211). The energy difference between the two adsorbed isomers (**Table 1**) is indeed the reaction energy difference between two possible dehydrogenation reactions of HCOOH, *viz.* HCOOH → HCOO + H and HCOOH → COOH + H. Hence, the general higher stability of HCOO than COOH on Au<sub>n</sub> clusters provides a first indication that the HCOO-mediated pathway might be more favorable than the COOH-mediated pathway in HCOOH decomposition on gold clusters. In the following sections, reaction pathway preference is further discussed based on results obtained from rigorous activation energy calculations.

### Activation energies for HCOOH dehydrogenation to HCOO on Au<sub>n</sub> (n=4-25) clusters

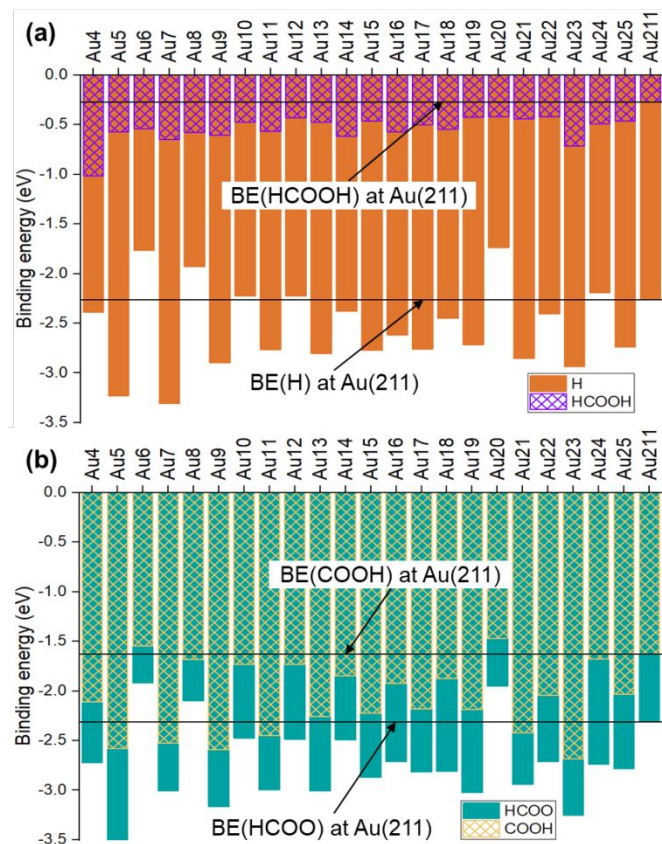


Figure 3 Binding energies of (a) H and HCOOH, (b) HCOO and COOH on Au<sub>n</sub> (n=4-25) clusters. Black horizontal lines show the corresponding BEs on Au(211). Energy zero refers to the respective adsorbate being at infinite separation from the cluster/surface.

In a previous work<sup>50</sup>, we studied the HCOOH decomposition reaction network with a total of 17 elementary steps, including HCOO, COOH as well as formyl (HCO) mediated decomposition pathways on three extended Au surfaces: (111), (100) and (211). HCOOH activation through C-OH bond scission forming HCO needs to come across very large barriers (> 1.7 eV) on all three Au surfaces, which makes the HCO-mediated route far less favorable than the other two decomposition routes. Although C-H scission in HCOOH to COOH is only slightly more activated (by 0.15 – 0.25 eV) than O-H scission in HCOOH to HCOO on the extended Au surfaces, it does not contribute to the reaction and the three-step HCOO-mediated pathway (HCOOH→HCOO+H; HCOO→CO<sub>2</sub>+H; H+H→H<sub>2</sub>) carries the entire reaction flux measured in experiments with Au catalyst dispersed on SiC. Both experimental and modeling results on the three Au surfaces show 100% selectivity towards dehydrogenation products, viz. CO is not formed during formic acid decomposition on Au.

As we discussed above, starting from HCOOH, HCOO formation is thermodynamically more favorable than COOH formation on

the Au<sub>n</sub> clusters studied in the present work, to a first approximation, we suggest that the three-step HCOO-mediated pathway (HCOOH→HCOO+H; HCOO→CO<sub>2</sub>+H; H+H→H<sub>2</sub>) might be the preferred decomposition path on Au<sub>n</sub> clusters as well. Accordingly, the first catalytic step in this pathway, viz. dehydrogenation of HCOOH to HCOO, was studied on Au<sub>n</sub> (n=4-25) clusters, and the calculated activation energies are used as a first criterion to screen Au<sub>n</sub> clusters that possess favorable properties for HCOOH decomposition. As Au(211) was found to be less active than the Au/SiC catalysts used in experiments by 5-6 orders of magnitude<sup>50</sup>, active Au<sub>n</sub> clusters should at least have a smaller barrier for HCOO formation than the one calculated on Au(211). Furthermore, in order to rationalize the experimentally measured reaction rates, the active Au site would need to possess an HCOO formation barrier which would be approximately 0.4-0.5 eV less than the corresponding value on Au(211).

We investigated HCOO formation on different sites of the Au<sub>n</sub> (n=4-25) clusters and the activation energy calculated in the minimum energy path found on each cluster are summarized in **Table 2**; the corresponding transition state (TS) configurations are shown in SI (**Figure S3**). We find that Au<sub>6</sub>, Au<sub>8</sub> and Au<sub>20</sub> have a higher (albeit not significantly higher) activation energy for HCOO formation than Au(211), which may partially originate from the weak interaction found between these three clusters and the relevant intermediates. This leads to elimination of these three clusters from further consideration to rationalize the experimental results. Au<sub>n</sub> clusters in the range n=9-16 and n=21-23 have similar activation energies for HCOO formation as Au(211) with very small differences of less than 0.20 eV being found. Thus, compared with the Au(211) surface, these clusters are expected to exhibit a similar or slightly higher reaction rates, which is far less than the 5-6 orders of magnitude rate increase required to represent the experimentally measured rates. As a result, Au<sub>n</sub> clusters in the range n=9-16 and n=21-23 are also ruled out from accurately describing the active site in the Au/SiC catalysts. Among the remaining Au<sub>n</sub> clusters, Au<sub>18</sub> has the lowest activation energy for HCOO formation, suggesting that Au<sub>18</sub> might be a promising model for the active site. In the following section, the other two steps in the HCOO-mediated pathway, and in some cases the COOH-mediated elementary reactions will be explored on clusters characterized with low HCOO formation barriers, specifically, Au<sub>4</sub>, Au<sub>5</sub>, Au<sub>7</sub>, Au<sub>17</sub>, Au<sub>18</sub> and Au<sub>19</sub>.

#### HCOOH decomposition on promising active site models (Au<sub>4</sub>, Au<sub>5</sub>, Au<sub>7</sub>, Au<sub>17</sub>-Au<sub>19</sub>)

Detailed reaction pathway studies were performed on the six Au<sub>n</sub> clusters (Au<sub>4</sub>, Au<sub>5</sub>, Au<sub>7</sub>, and Au<sub>17</sub>-Au<sub>19</sub>) identified as promising models for the active site in the Au/SiC catalysts evaluated experimentally in our previous work.<sup>50</sup> The kinetically relevant HCOO pathway (found on extended Au

surfaces) comprised of three elementary steps (reactions 2-4 in **Table 3**) was investigated on all six clusters. To ensure that we are not biasing our mechanistic understanding against the COOH-mediated pathway, the elementary reactions in this pathway (reactions 5-10 in **Table 3**) were also calculated on four clusters ( $\text{Au}_5$ ,  $\text{Au}_7$ ,  $\text{Au}_{18}$  and  $\text{Au}_{19}$ ); as we will show later, the COOH pathway was found to be irrelevant for HCOOH decomposition on these four clusters and therefore was not studied on the remaining two clusters. The calculated activation energies and reaction energies on the six gold clusters are summarized in **Table 3**.

#### HCOOH decomposition on $\text{Au}_4$

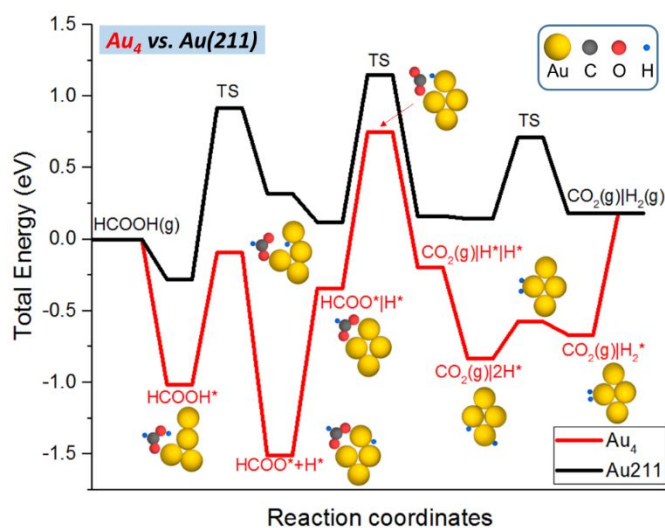


Figure 4 Potential energy diagram (PED) of HCOOH decomposition through the HCOO pathway on  $\text{Au}_4$ . PED for  $\text{Au}(211)$  is shown in black line for comparison. Insets show configurations of the most favorable adsorbed states and transition states on  $\text{Au}_4$ . ‘|’ indicates infinite separation, while ‘+’ indicates the intermediates are co-adsorbed on the surface/cluster. The same notation is adopted throughout this work.

On  $\text{Au}_4$ , an exceptionally strong BE of HCOOH is found, -1.02 eV; along with the adsorption of HCOOH,  $\text{Au}_4$  undergoes a structural transformation from the most stable rhombic structure (see **Figure 1**) to a ‘Y-shaped’ structure (see inset in **Figure 4** for  $\text{HCOOH}^*$ ). Further structural rearrangement is observed during the dehydrogenation of HCOOH to HCOO, bringing  $\text{Au}_4$  back to its original rhombic structure, with the HCOO bound in a bidentate top-top mode on one side of the rhombus and H sitting at the nearest bridge site. HCOOH dehydrogenation to co-adsorbed HCOO and H is an exothermic reaction with a barrier of 0.92 eV. Co-adsorbed HCOO and H intermediates on  $\text{Au}_4$  possess a significantly attractive interaction of 1.17 eV. Further dehydrogenation of HCOO involves flipping and rotation of HCOO to first break one O-Au bond, leading to a structure with its C-H bond pointing towards the cluster. The C-H bond in that structure is readily broken in a subsequent, close-to-spontaneous, step. The overall barrier required for HCOO decomposition on  $\text{Au}_4$  is 1.09 eV. Combination of two co-adsorbed and attractively interacting H atoms (by 0.64 eV) easily forms a molecularly adsorbed  $\text{H}_2$  state, which binds to  $\text{Au}_4$  with -0.70 eV.

Comparing the potential energy diagram (PED) of the HCOO pathway on  $\text{Au}_4$  with that on the  $\text{Au}(211)$  surface (**Figure 4**), we observe that the TSs of the three elementary steps are substantially stabilized on  $\text{Au}_4$  compared to  $\text{Au}(211)$ , primarily because of the significantly stronger interactions of the intermediates with  $\text{Au}_4$ . Importantly, when HCOO (or H) is co-adsorbed with another H on  $\text{Au}_4$ , the co-adsorption state is stabilized by 1.17 eV (or 0.64 eV) compared with the infinite-separation counterpart, forming a deep potential well on the PED. This may imply that  $\text{Au}_4$  is partially covered with HCOO and (or) H species. Furthermore, desorption of molecular hydrogen is an energetically demanding step characterized by a desorption energy of 0.70 eV, while  $\text{H}_2$  dissociation into atomic hydrogen has only a negligible barrier of 0.09 eV, further suggesting that  $\text{Au}_4$  may be partially covered by atomic H during reaction.

#### HCOOH decomposition on $\text{Au}_5$ and $\text{Au}_7$

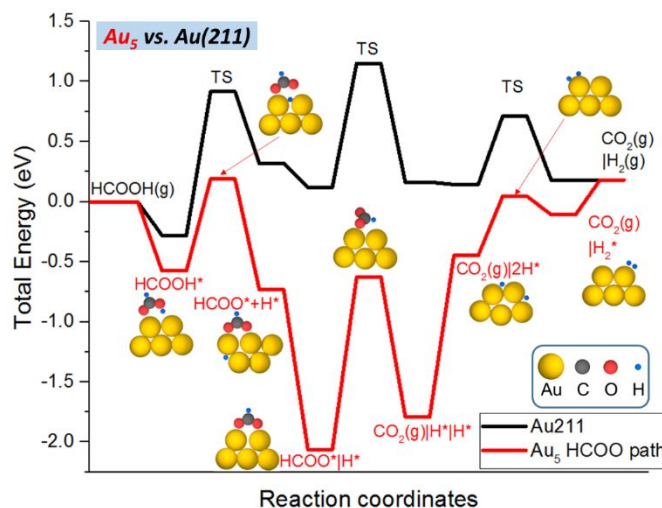


Figure 5 Potential energy diagram (PED) of HCOOH decomposition through the HCOO pathway on  $\text{Au}_5$ . PED for  $\text{Au}(211)$  is shown in black line for comparison.

On  $\text{Au}_5$ , HCOOH adsorbs on the shorter parallel side of the trapezoid (**Figure 5**) with a BE of -0.58 eV. Its dehydrogenation has a modest barrier of 0.76 eV, forming HCOO adsorbed on two Au sites of the longer parallel edge of  $\text{Au}_5$  with H bound to a nearby bridge side. Contrary to the case of  $\text{Au}_4$ , on  $\text{Au}_5$  a strong repulsive interaction between co-adsorbed HCOO and H is observed, leading to a deep potential well for the two adsorbed species at infinite separation. Though subsequent HCOO decomposition has a very high barrier of 1.44 eV, its TS lies below the other two TSs in the HCOO pathway due to the low-lying initial state.  $\text{H}_2$  formation needs to first overcome the repulsion (of 1.34 eV) between two hydrogen atoms on  $\text{Au}_5$  and then come across a barrier of 0.49 eV to form the H-H bond at the vertex of the shorter parallel edge. Thus, an overall barrier 1.83 eV is associated with  $\text{H}_2$  formation on  $\text{Au}_5$ , which may represent the rate-limiting step (RLS) and imply an H-covered site environment. Compared to  $\text{Au}(211)$ , the PED on  $\text{Au}_5$  (**Figure 5**) is significantly shifted to lower energies, due to

the observed stabilization of various intermediates (HCOOH, HCOO and H).

The COOH-mediated pathway leading to either CO<sub>2</sub> (COOH-CO<sub>2</sub> path) or CO production (COOH-CO path) was also investigated on Au<sub>5</sub>. We found that COOH formation is more difficult than HCOO formation, and COOH dehydrogenation has a higher TS energy than HCOO dehydrogenation on Au<sub>5</sub>. Though COOH decomposition to CO is relatively easy, water formation in the COOH-CO path is characterized by a high-energy TS, which is much higher in energy than the highest TS in the HCOO pathway. Hence, the COOH-mediated pathway is less preferred compared to the HCOO pathway on Au<sub>5</sub>. The two pathways can be directly compared in **Figure S4**.

Au<sub>7</sub> shows very similar catalytic properties for HCOOH decomposition to those of Au<sub>5</sub>; **Figure S5** shows the nearly identical PEDs on the two clusters. The only dramatic difference observed is that HCOO binds much stronger to Au<sub>5</sub> than to Au<sub>7</sub>. Again, on Au<sub>7</sub> the HCOO pathway is more favorable than the COOH pathway (**Figure S6**). Like the case on Au<sub>5</sub>, on Au<sub>7</sub>, we expect recombinative desorption of hydrogen to be the rate limiting step for formic acid decomposition.

#### Interaction energy between co-adsorbed intermediates

We noticed from the above discussions that, the interaction energy between co-adsorbed intermediates varies dramatically with different sized Au<sub>n</sub> clusters, resulting in quite different potential energy diagrams for HCOOH decomposition. Table 4 summarizes the interaction energy between H and HCOO and H and H on the six promising Au<sub>n</sub> (Au<sub>4</sub>, Au<sub>5</sub>, Au<sub>7</sub> and Au<sub>17</sub>-Au<sub>19</sub>) cluster; the former was also calculated on other Au<sub>n</sub> clusters in the range n=4-25 (see **Figure S7**). Again, a striking odd-even alternation is observed: odd-numbered Au<sub>n</sub> clusters exhibit strong repulsive interaction between co-adsorbed H and HCOO as well as H and H, while even-numbered Au<sub>n</sub> clusters show attractive coadsorption. This could be explained in a simple valence electron structure model that odd-numbered gold clusters with preadsorbed H (or HCOO) have a closed-shell valence electronic structure leading to a lower binding energy for the adsorption of an additional H atom (that is, repulsive interaction would be seen for co-adsorbed H or HCOO with H), while even-numbered gold clusters with preadsorbed H (or HCOO) possess an unpaired valence electron that may promote further H adsorption to pair that electron. A similar phenomenon has also been reported for coadsorption of H<sub>2</sub> and O<sub>2</sub> on gold cations by Landman and coworkers<sup>83</sup>. The interaction between H and HCOO or H on Au<sub>17</sub> and Au<sub>18</sub> has a modest strength of ca. 0.2-0.4 eV (either repulsive or attractive, respectively), which is much weaker than those on the other four clusters. As strong interactions between co-adsorbed intermediates will lead to either deep potential wells or high potential peaks on the PED that are not characteristics of good catalytic performance, Au<sub>17</sub> and Au<sub>18</sub> might be more appropriate

representations of the active site. HCOOH decomposition on these two gold clusters are discussed in the next section.

#### HCOOH decomposition on Au<sub>17</sub>-Au<sub>19</sub>

As suggested earlier, the structures of Au<sub>17</sub>, Au<sub>18</sub>, Au<sub>19</sub> can be obtained by removing three, two and one vertex Au atom(s) from the Au<sub>20</sub> pyramid, and thereby exposing three, two and one ensemble(s) of Au<sub>3</sub> triangular site(s), all marked by the pink atoms in **Figure 6**, respectively. Atoms on the Au<sub>3</sub> sites are highly under-coordinated with a CN of 5. As we will suggest later in the discussion, these triangular Au<sub>3</sub> sites are the main active sites for formic acid decomposition on all three gold clusters Au<sub>17</sub>-Au<sub>19</sub>. Such triangular sites have also been reported to be the main active sites for CO oxidation on monometallic nanosized Au<sup>84</sup>, Cu clusters<sup>85</sup>, and bimetallic clusters<sup>86-88</sup>, as well as the styrene epoxidation and oxidation reactions on Au clusters<sup>89</sup>.

Au<sub>17</sub> and Au<sub>19</sub> are two cluster models that are more reactive than Au(211), observed from the lower-lying PED on the two clusters compared with the PED on Au(211) (**Figure 7 and 8**). The three catalytic steps occur exclusively on the triangular Au<sub>3</sub> sites of both clusters. Due to the repulsive interactions of co-adsorbed HCOO (or H) with H on these two odd-numbered clusters, the third step – hydrogen recombination – has the highest TS energy among the three steps.

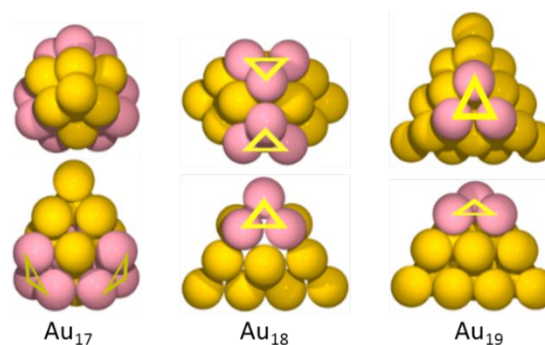


Figure 6 Minimum energy structures for Au<sub>17</sub>, Au<sub>18</sub> and Au<sub>19</sub>. Pink atoms and the yellow triangles connecting them indicate the triangular Au<sub>3</sub> sites with CN of 5.

Au<sub>18</sub>, an even-numbered cluster, has modest attractive interactions between co-adsorbed HCOO (or H) with H, rendering the 2<sup>nd</sup> TS – decomposition of HCOO – possessing the highest energy among the three TSs and potentially being the RLS (**Figure 9**). Similar to the case of Au<sub>17</sub> and Au<sub>19</sub>, the triangular Au<sub>3</sub> sites with CN of 5 are also the dominant active sites on Au<sub>18</sub>. Comparing the PEDs on the three Au clusters exposing the triangular Au<sub>3</sub> sites, the catalytic activities of the three clusters for HCOOH decomposition are expected to be different, mainly due to the electronic effect rather than geometric effect.

The COOH pathway was also explored on Au<sub>18</sub> and Au<sub>19</sub>. PEDs comparing the COOH pathway with the HCOO pathway on the

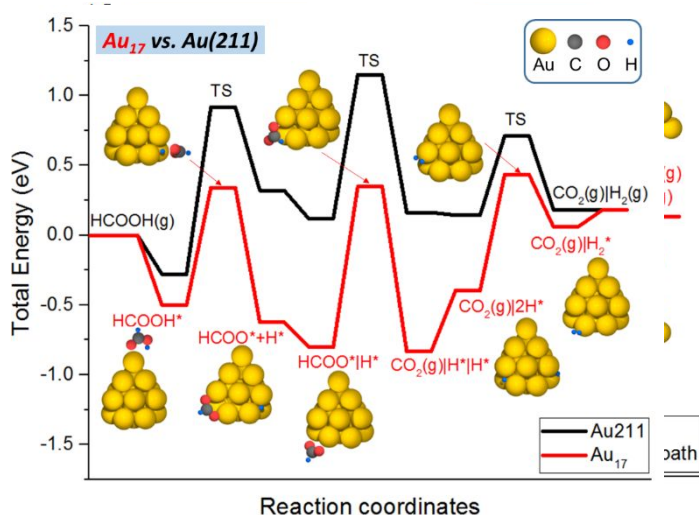


Figure 7 Potential energy diagram (PED) of HCOOH decomposition through the HCOO path on Au<sub>17</sub>. PED for Au(211) is shown in black line, for comparison.

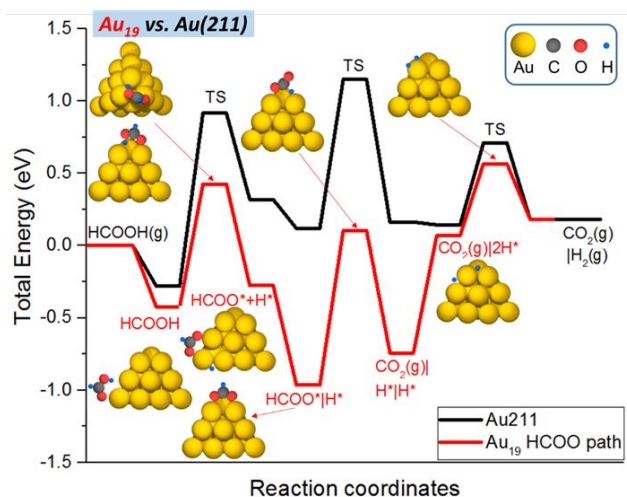


Figure 8 Potential energy diagram (PED) of HCOOH decomposition through the HCOO path on Au<sub>19</sub>. PED for Au(211) is shown in black line, for

two clusters (see Figures S8 and S9) show that the latter is preferred for formic acid decomposition on Au<sub>18</sub> and Au<sub>19</sub>.

Based on the above results, all six gold clusters (Au<sub>4</sub>, Au<sub>5</sub>, Au<sub>7</sub>, Au<sub>17</sub>–Au<sub>19</sub>) on which the complete catalytic cycle for HCOOH decomposition was examined are more reactive than Au(211). From the respective PEDs, we tend to conclude that the reaction proceeds preferentially through the HCOO-mediated path, same as on the extended surfaces of Au (Au(111), Au(100) and Au(211)) studied previously.<sup>50</sup> To determine which of these clusters may better represent the active site of the Au/SiC catalysts used in our experiments for HCOOH decomposition, a microkinetic modeling analysis was conducted to compare the DFT results with the experimental results. This analysis will be presented in the next section.

#### Microkinetic modeling

DFT-derived parameters on each of the six Au<sub>n</sub> clusters discussed above were used as the input of microkinetic model to fit our earlier experimental data<sup>50</sup>. By adjusting the DFT obtained parameters, we could get a good fit with the experimental results (with mean absolute errors of less than 15%). Adjustments needed for the six Au<sub>n</sub> clusters are summarized in **Table 5**, together with the surface coverage predicted from the model after adopting these adjustments. Parity plot comparing the experimental conversion and model-predicted conversion obtained with adjusted parameters on Au<sub>18</sub> is shown in **Figure S11**.

On the Au clusters where the CO formation pathway was explored, similar to what we found on the extended Au surfaces, the reaction proceeds solely through the HCOO-mediated pathway with 100% selectivity towards hydrogen. In general, to obtain a good fit with the experimental results, destabilization in H adsorption is required on all six gold clusters except for Au<sub>18</sub>; especially on Au<sub>5</sub> and Au<sub>7</sub>, H adsorption has to be significantly destabilized by 0.62 eV and

0.81 eV, respectively, which confirms our earlier hypothesis that a H-covered surface is expected for Au<sub>5</sub> and Au<sub>7</sub> and H recombination might be the rate limiting step on these two clusters. On Au<sub>4</sub>, H has to be destabilized by 0.41 eV, while the TS of HCOO decomposition had to be stabilized by 0.51 eV, which is the largest adjustment needed on Au<sub>4</sub>. To obtain a good fit on Au<sub>17</sub>–Au<sub>19</sub>, the TSs of the three elementary steps had to be stabilized by ca. 0.1–0.4 eV. The adjustments required for parameters derived on Au<sub>17</sub>–Au<sub>19</sub> are much smaller than those needed on the three smaller clusters Au<sub>4</sub>, Au<sub>5</sub> and Au<sub>7</sub>, suggesting that Au<sub>4</sub>, Au<sub>5</sub> and Au<sub>7</sub> are less likely to be the active site for HCOOH decomposition. On all six clusters, the surface is expected to be covered mainly by HCOO (with a coverage of up to 0.58 ML on Au<sub>5</sub>) except for Au<sub>4</sub>, which is covered by 0.04–0.40 ML of HCOOH resulting from the particularly strong binding of HCOOH (BE is -1.02 eV) on Au<sub>4</sub>. H is predicted to occupy only less than 0.01 ML of the surface sites of all clusters studied.

Among the six clusters studied, Au<sub>18</sub> is characterized by the smallest adjustments required to obtain a good fit to our previous experimental data, and therefore appears to be the most promising cluster model for representing the nature of the active site for HCOOH decomposition. On Au<sub>18</sub>, the largest adjustment needed is for the TS of HCOO decomposition, which needs to be stabilized by 0.29 eV, while all the other adjustments made were smaller than 0.2 eV, within the error of our DFT calculations. While the 0.29 eV stabilization on the TS of HCOO decomposition exceeds the DFT error bar, we note here that van der Waals interactions were not accounted for in this work. To probe this effect, we calculated the BE of HCOO on Au<sub>18</sub> by including van der Waals interactions, and found an enhanced binding by 0.22 eV, which would bring a stabilization of about the same amount to the TS of HCOO decomposition; that would then be very close to the 0.29 eV stabilization determined through our microkinetic model. Similar arguments can be made for the TSs on Au<sub>17</sub> and Au<sub>19</sub> since the adjustments needed there were similar to those on Au<sub>18</sub>. However, on these two clusters H binding should also be weakened by 0.2–0.3 eV, whereas van der Waals interactions would lead to a stronger binding of H by 0.17 eV. This suggests that an even larger adjustment to the binding of H on Au<sub>17</sub> and Au<sub>19</sub> would be needed to capture the experimental data, rendering Au<sub>17</sub> and Au<sub>19</sub> less realistic representations of the active site present in experiments.

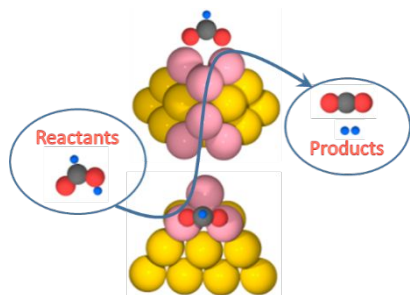


Figure 9 Schematic illustration of the HCOOH decomposition process on Au<sub>18</sub>. Au, C, O and H atoms are represented by the yellow, grey, red and blue circles. The triangular Au<sub>3</sub> site on Au<sub>18</sub> is indicated by the pink circles.

Based on the DFT-informed microkinetic modeling results, we conclude that Au<sub>18</sub> is the most realistic representation of the active site for HCOOH decomposition on Au/SiC catalysts. On Au<sub>18</sub>, HCOOH decomposes through the HCOO intermediate at the triangular Au<sub>3</sub> site where each Au atom has a CN=5 (**Figure 14**). Even though, Au<sub>17</sub> and Au<sub>19</sub> have similar Au<sub>3</sub> sites, they are not accurate representations of the active site, simply because of the magnitude of the parameter adjustment needed to capture the experimental data. Therefore, even a single atom of Au can make a big difference in the activity of Au<sub>n</sub> clusters. This effect on the activity of sub-nanometer scale clusters is not confined to formic acid decomposition. It has also been reported for other reactions, including CO oxidation<sup>90–93</sup> and the oxygen reduction reaction<sup>94–96</sup> on transition metal clusters. Recent advances in atomically precise synthesis<sup>97–101</sup> of subnanometric metal clusters can enable the synthesis of mass-selected Au nanoclusters, which could be very efficient catalysts for various reactions, including formic acid decomposition to CO<sub>2</sub> and H<sub>2</sub>.

We note that the support effect is not considered in our calculations, mainly because the SiC support used in experiments is inert for formic acid decomposition. Nevertheless, SiC support may play a role in determining the catalytic performance of gold catalysts by either changing the geometry of the Au clusters or by creating unique sites at the Au–SiC interface. On different support materials, the intrinsic activity can vary dramatically. Some metal oxide supports (e.g. Al<sub>2</sub>O<sub>3</sub>, CeO<sub>2</sub> etc.) are able to activate formic acid; in such scenario, the catalytic activity will be strongly affected by the acid-base properties of the support.<sup>102</sup> Porous materials could also influence the catalytic activity by controlling the size and essentially adjusting the number of low-coordinated sites of encapsulated gold nanoparticles.<sup>103</sup> While we focused on the size effect of Au clusters on their catalytic properties and identified notable atomic-scale size-sensitivity in formic acid decomposition in this work, future studies may need to take into account other factors (e.g. the support effects) in order to develop a more comprehensive understanding of the catalytic activity of supported gold clusters for this reaction.

## Conclusions

*Ab initio* molecular dynamics simulations were performed for sub-nanometer gold clusters (up to Au<sub>25</sub> with a size of 0.85 nm) to determine their most stable structures. Subsequently, on these structures, the formic acid decomposition was systematically studied using DFT calculations. The DFT derived parameters were then used in a microkinetic model to compare against experimental results on Au/SiC catalysts and to infer the most likely nature of the active site for this reaction system.

The DFT results suggest that planar structures are preferred for small gold clusters, with the 2D-to-3D transition taking place at Au<sub>17</sub>. An odd-even oscillation is seen for the differential binding energy of Au in Au<sub>n</sub> clusters and the binding energies of reactive intermediates. Odd-numbered Au clusters bind these open-shell (e.g. H and HCOO) intermediates

more strongly than their neighboring even-numbered  $Au_n$  clusters. Strongly repulsive interactions between H and HCOO (or H) are observed on odd-numbered Au clusters while the interactions are attractive on even-numbered clusters. All the clusters studied here show stronger binding for the intermediates than Au(211), except  $Au_6$ ,  $Au_8$  and  $Au_{20}$ , due to the high stabilities resulted from the high symmetries found in their structures. This is a first indication that sub-nanometer gold clusters might be more reactive than Au(211) and potentially serve as the active site for HCOOH decomposition on Au/SiC.

HCOOH dehydrogenation, as the first step in formic acid decomposition, was studied on  $Au_4$ - $Au_{25}$ . Based on the comparison of the activation energies of this step with that on the Au(211) surface, a subset of the  $Au_n$  clusters were identified for further studies:  $Au_4$ ,  $Au_5$ ,  $Au_7$  and  $Au_{17}$ - $Au_{19}$ . A comprehensive DFT study of the elementary reaction steps on these six clusters was then conducted, including not only the HCOO-mediated route suggested as the preferred pathway by previous studies, but also the COOH-mediated route. We found that the HCOO-mediated path is much more energetically preferable than the COOH-mediated path on these Au clusters.

In a final step, a mean-field microkinetic model was used to fit the DFT derived BEs of the intermediates and activation energies of the elementary steps on the six gold clusters, to match the experimentally measured reaction rate. The parameter adjustment results suggest that among the six gold clusters,  $Au_{18}$  is the most accurate representation of the active site for HCOOH decomposition on Au/SiC. Only small adjustments, within the DFT error bars, were required in order to obtain a good fit with the experimental data. On  $Au_{18}$ , the reaction proceeds via the HCOO intermediate on a triangular  $Au_3$  site with a coordination number of 5 for the relevant Au atoms. Though, the same  $Au_3$  site is also present on  $Au_{17}$  and  $Au_{19}$ , the large adjustments needed in fitting the experimental rates suggest that  $Au_{17}$  and  $Au_{19}$  may not be accurate representations of the active site for this reaction system. Therefore, we have demonstrated an atomic scale size-sensitivity of the catalytic properties of sub-nanometer gold clusters for HCOOH decomposition. To assess the importance of discrete reaction events in understanding this catalytic system, current studies in our group explore stochastic modeling methods (e.g. kinetic Monte Carlo) in place of the mean-field microkinetic model described here. These stochastic methods allow for the inclusion of detailed site-resolved lateral interactions between adsorbates and can potentially give a more accurate description of reaction kinetics on small catalytic clusters.

## Computational Methods

All calculations were performed using the Vienna *ab initio* simulation package (VASP) code<sup>104, 105</sup> based on density functional theory (DFT). The projector augmented wave (PAW)<sup>106, 107</sup> potentials were used for electron-ion interactions, and the generalized gradient approximation

(GGA-PW91)<sup>108</sup> was used to describe the exchange-correlation functional. The electron wave function was expanded using plane waves with an energy cutoff of 400 eV. All calculations were performed in a  $20 \times 20 \times 20 \text{ \AA}^3$  cubic cell with 3-dimensional periodic boundary conditions and the Brillouin zone were sampled by the gamma point only. The vdW-DF based optPBE-vdW functional developed by Michaelides and co-workers<sup>109, 110</sup> was used to estimate the effect of dispersion interactions.

To obtain the most stable configurations of the Au clusters, DFT calculations were performed in the framework of *ab-initio* molecular dynamics (AIMD)<sup>111</sup>. First, several initial guesses of cluster models were statically optimized to local minima, which subsequently underwent AIMD simulated annealing. In the simulated annealing, the system was first equilibrated at a high temperature (550K) for 2 ps, then quenched to room temperature within 2 ps, and finally, the local minima of the quenching trajectory were statically optimized to yield final structures. From these local minima, the most stable one for a given  $Au_n$  cluster was chosen as the optimized structure.

During the structure optimization of the adsorbates and activation energy calculations on Au clusters, all Au atoms were fully relaxed. Structures were fully relaxed until the Hellmann-Feynman forces acting on the atoms were smaller than  $0.02 \text{ eV/\AA}$ . Binding energy (BE) of the adsorbate/intermediate was calculated with respect to the pure Au cluster and the corresponding adsorbate/intermediate at infinite separation between each other in the gas phase. Minimum energy paths and activation energy barriers of the elementary steps were calculated using the climbing image nudged elastic band method (CI-NEB)<sup>112</sup>. The minimum energy path for each elementary step was discretized by a total of at least nine images, including the initial and final states. Convergence of the NEB calculations was reached when the magnitude of the force on all images was less than  $0.1 \text{ eV/\AA}$ , except for the hydrogen recombination reaction, where a stricter convergence criterion ( $0.05 \text{ eV/\AA}$ ) was used. The transition states (TS) were confirmed by vibrational frequency calculations yielding a single imaginary frequency along the reaction coordinate. DFT results on the Au(211) surface presented in this work are taken from our previous publication.<sup>50</sup>

Reaction kinetics data for formic acid decomposition was collected on a Au/SiC catalyst in the temperature range of 343-383K and was imported into a microkinetic model developed on the basis of the eleven elementary steps given in Table 3. Following a procedure described elsewhere<sup>113</sup>, DFT-calculated vibrational frequencies on the intermediates and transition states allows the calculation of rate constants of all elementary reactions via harmonic transition state theory. These rate constants were used to solve a set of coupled differential rate equations to determine the surface coverage and the overall reaction rate. DFT-derived BE and  $E_a$  parameters were then adjusted in a systematic way until reasonable agreement between the experimental and model predicted reaction rates was reached; Table 5 lists the parameters adjustments needed for the best-fitted solution. Lateral adsorbate-adsorbate interactions were neglected in our mean-field microkinetic

model and the BE and Ea parameters were assumed to be coverage independent. Microkinetic models including detailed site-specific lateral interactions would improve the accuracy of predictions of reaction kinetics on small clusters, but this is beyond the scope of this work. Reaction kinetics data and details of the experimental methods and microkinetic modeling have been reported and can be found in a previous publication<sup>50</sup>.

### Conflicts of interest

There are no conflicts to declare.

### Acknowledgements

This work was supported by the U.S. Department of Energy (DOE)–Basic Energy Sciences (BES), Office of Chemical Sciences, grant DE-FG02-05ER15731. Calculations were performed at supercomputing centers located at the Environmental Molecular Sciences Laboratory, which is sponsored by the DOE Office of Biological and Environmental Research at the Pacific Northwest National Laboratory; Center for Nanoscale Materials at Argonne National Laboratory, supported by DOE contract DE-AC02-06CH11357; and National Energy Research Scientific Computing Center, supported by DOE contract DE-AC02-05CH11231. We thank Lang Xu and Benjamin Chen for providing valuable comments on the manuscript.

### Notes and references

- 1 M. Haruta, N. Yamada, T. Kobayashi and S. Iijima, *J. Catal.*, 1989, **115**, 301-309.
- 2 M. Haruta, T. Kobayashi, H. Sano and N. Yamada, *Chem. Lett.*, 1987, **2**, 405-408.
- 3 M. Haruta, *Chem. Rec.* 2003, **3**, 75-87.
- 4 Q. Liu, X. Yang, Y. Huang, S. Xu, X. Su, X. Pan, J. Xu, A. Wang, C. Liang, X. Wang and T. Zhang, *Energy Environ. Sci.*, 2015, **8**, 3204-3207.
- 5 J. Gong, *Chem. Rev.*, 2012, **112**, 2987-3054.
- 6 G. J. Hutchings, M. Brust and H. Schmidbaur, *Chem. Soc. Rev.*, 2008, **37**, 1759-1765.
- 7 G. J. Hutchings and M. Haruta, *Appl. Catal. A*, 2005, **291**, 2-5.
- 8 L. Li, Y. Gao, H. Li, Y. Zhao, Y. Pei, Z. Chen and X. C. Zeng, *J. Am. Chem. Soc.*, 2013, **135**, 19336-19346.
- 9 J. Saavedra, H. A. Doan, C. J. Pursell, L. C. Grabow and B. D. Chandler, *Science*, 2014, **345**, 1599-1602.
- 10 H. Falsig, B. Hvolbæk, I. S. Kristensen, T. Jiang, T. Bligaard, C. H. Christensen and J. K. Nørskov, *Angew. Chem. Int. Ed.*, 2008, **47**, 4835-4839.
- 11 N. Lopez, T. V. W. Janssens, B. S. Clausen, Y. Xu, M. Mavrikakis and J. K. Nørskov, *J. Catal.*, 2004, **223**, 232-235.
- 12 I. Remediakis, N. Lopez and J. K. Nørskov, *Angew. Chem. Int. Ed.*, 2005, **44**, 1824-1826.
- 13 L. M. Molina, M. D. Rasmussen and B. Hammer, *J. Chem. Phys.*, 2004, **120**, 7673-7680.
- 14 D. Widmann and R. J. Behm, *Acc. Chem. Res.*, 2014, **47**, 740-749.
- 15 M. S. Ide and R. J. Davis, *Acc. Chem. Res.*, 2014, **47**, 825-833.
- 16 A. Taketoshi and M. Haruta, *Chem. Lett.*, 2014, **43**, 380-387.
- 17 M. Haruta and M. Date, *Appl. Catal. A*, 2001, **222**, 427-437.
- 18 B. Hvolbæk, T. V. W. Janssens, B. S. Clausen, H. Falsig, C. H. Christensen and J. K. Nørskov, *Nano Today*, 2007, **2**, 14-18.
- 19 B. K. Min and C. M. Friend, *Chem. Rev.*, 2007, **107**, 2709-2724.
- 20 I. N. Remediakis, N. Lopez and J. K. Nørskov, *Appl. Catal. A*, 2005, **291**, 13-20.
- 21 L. M. Molina and B. Hammer, *Appl. Catal. A*, 2005, **291**, 21-31.
- 22 K. J. Hu, S. R. Plant, P. R. Ellis, C. M. Brown, P. T. Bishop and R. E. Palmer, *J. Am. Chem. Soc.*, 2015, **137**, 15161-15168.
- 23 H. M. Ajo, V. A. Bondzie and C. T. Campbell, *Catal. Lett.*, 2002, **78**, 359-368.
- 24 A. K. Sinha, S. Seelan, S. Tsubota and M. Haruta, *Top. Catal.*, 2004, **29**, 95-102.
- 25 B. Taylor, J. Lauterbach and W. N. Delgass, *Appl. Catal. A*, 2005, **291**, 188-198.
- 26 M. Flytzani-Stephanopoulos, *Acc. Chem. Res.*, 2014, **47**, 783-792.
- 27 M. Yang, L. F. Allard and M. Flytzani-Stephanopoulos, *J. Am. Chem. Soc.*, 2013, **135**, 3768-3771.
- 28 W. Deng, A. I. Frenkel, R. Si and M. Flytzani-Stephanopoulos, *J. Phys. Chem. C*, 2008, **112**, 12834-12840.
- 29 N. Yi, R. Si, H. Saltsburg and M. Flytzani-Stephanopoulos, *Energy Environ. Sci.*, 2010, **3**, 831-837.
- 30 M. Shekhar, J. Wang, W. S. Lee, M. C. Akatay, E. A. Stach, W. N. Delgass and F. H. Ribeiro, *J. Catal.*, 2012, **293**, 94-102.
- 31 M. Shekhar, J. Wang, W. S. Lee, W. D. Williams, S. M. Kim, E. A. Stach, J. T. Miller, W. N. Delgass and F. H. Ribeiro, *J. Am. Chem. Soc.*, 2012, **134**, 4700-4708.
- 32 W. D. Williams, M. Shekhar, W. S. Lee, V. Kispersky, W. N. Delgass, F. H. Ribeiro, S. M. Kim, E. A. Stach, J. T. Miller and L. F. Allard, *J. Am. Chem. Soc.*, 2010, **132**, 14018-14020.
- 33 Z. Xu, F. S. Xiao, S. K. Purnell, O. Alexeev, S. Kawi, S. E. Deutsch and B. C. Gates, *Nature*, 1994, **372**, 346-348.
- 34 J. F. Jia, K. Haraki, J. N. Kondo, K. Domen and K. Tamaru, *J. Phys. Chem. B*, 2000, **104**, 11153-11156.
- 35 J. A. Lopez-Sanchez and D. Lennon, *Appl. Catal. A*, 2005, **291**, 230-237.
- 36 N. Yi, H. Saltsburg and M. Flytzani-Stephanopoulos, *ChemSusChem*, 2013, **6**, 816-819.
- 37 M. Ojeda and E. Iglesia, *Angew. Chem. Int. Ed.*, 2009, **48**, 4800-4803.
- 38 A. Gazsi, T. Bansagi and F. Solymosi, *J. Phys. Chem. C*, 2011, **115**, 15459-15466.
- 39 D. A. Bulushev, S. Beloshapkin and J. R. H. Ross, *Catal. Today*, 2010, **154**, 7-12.
- 40 J. S. Yoo, F. Abild-Pedersen, J. K. Nørskov and F. Studt, *ACS Catal.*, 2014, **4**, 1226-1233.

- 41 J. A. Herron, J. Scaranto, P. Ferrin, S. Li and M. Mavrikakis, *ACS Catal.*, 2014, **4**, 4434-4445.
- 42 D. Tibiletti, A. Amieiro-Fonseca, R. Burch, Y. Chen, J. M. Fisher, A. Goguet, C. Hardacre, P. Hu and D. Thompsett, *J. Phys. Chem. B*, 2005, **109**, 22553-22559.
- 43 D. Andreeva, *Gold Bull.*, 2002, **35**, 82-88.
- 44 Q. Y. Bi, X. L. Du, Y. M. Liu, Y. Gao, H. Y. He and K. N. Fan, *J. Am. Chem. Soc.*, 2012, **134**, 8926-8933.
- 45 D. J. Braden, C. A. Henao, J. Heltzel, C. T. Maravelias and J. A. Dumesic, *Green Chem.*, 2011, **13**, 1755-1765.
- 46 J. C. Serrano-Ruiz, D. J. Braden, R. M. West and J. A. Dumesic, *Appl. Catal. B*, 2010, **100**, 184-189.
- 47 J. Q. Bond, D. M. Alonso, D. Wang, R. M. West and J. A. Dumesic, *Science*, 2010, **327**, 1110-1114.
- 48 F. Solymosi, A. Koos, N. Liliom and I. Ugrai, *J. Catal.*, 2011, **279**, 213-219.
- 49 D. A. Bulushev, L. G. Bulusheva, S. Beloshapkin, T. O'Connor, A. V. Okotub and K. M. Ryan, *ACS Appl. Mater. Interfaces*, 2015, **7**, 8719-8726.
- 50 S. Singh, S. Li, R. Carrasquillo-Flores, A. C. Rlba-Rubio, J. A. Dumesic and M. Mavrikakis, *AIChE J.*, 2014, **60**, 1303-1319.
- 51 P. Gruene, B. Butschke, J. T. Lyon, D. M. Rayner and A. Fielicke, *Z. Phys. Chem. (Muenchen, Ger.)*, 2014, **228**, 337-350.
- 52 Y. D. Li and Y. Gao, *Chin. Sci. Bull.*, 2014, **59**, 239-246.
- 53 D. Schooss, P. Weis, O. Hampe and M. M. Kappes, *Philos. Trans. R. Soc. A*, 2010, **368**, 1211-1243.
- 54 A. P. Woodham and A. Fielicke, *Gold Clusters, Colloids and Nanoparticles I*, Springer, Cham, 2014.
- 55 Y. Gao, N. Shao, Y. Pei, Z. Chen and X. C. Zeng, *ACS Nano*, 2011, **5**, 7818-7829.
- 56 F. Furche, R. Ahlrichs, P. Weis, C. Jacob, S. Gilb, T. Bierweiler and M. M. Kappes, *J. Chem. Phys.*, 2002, **117**, 6982-6990.
- 57 M. P. Johansson, A. Lechtken, D. Schooss, M. M. Kappes and F. Furche, *Phys. Rev. A*, 2008, **77**, 053202.
- 58 X. Xiaopeng, Y. Bokwon, U. Landman and J. H. Parks, *Phys. Rev. B*, 2006, **74**, 165423.
- 59 A. Lechtken, C. Neiss, M. M. Kappes and D. Schooss, *Phys. Chem. Chem. Phys.*, 2009, **11**, 4344-4350.
- 60 P. Gruene, D. M. Rayner, B. Redlich, A. F. G. van der Meer, J. T. Lyon, G. Meijer and M. Fielicke, *Science*, 2008, **321**, 674-676.
- 61 H. Häkkinen, B. Yoon and U. Landman, *J. Phys. Chem. A*, 2003, **107**, 6168-6175.
- 62 B. Yoon, P. Koskinen, B. Huber, O. Kostko, B. von Issendorff, H. Häkkinen, M. Moseler and U. Landman, *ChemPhysChem*, 2007, **8**, 157-161.
- 63 J. Li, X. Li, H. J. Zhai and L. S. Wang, *Science*, 2003, **299**, 864-867.
- 64 W. Huang, S. Bulusu, R. Pal, X. C. Zeng and L. S. Wang, *ACS Nano*, 2009, **3**, 1225-1230.
- 65 S. Bulusu, X. Li, L. S. Wang and X. C. Zeng, *J. Phys. Chem. C*, 2007, **111**, 4190-4198.
- 66 J. Wang, G. Wang and J. Zhao, *Phys. Rev. B*, 2002, **66**, 035418.
- 67 L. M. Wang and L. S. Wang, *Nanoscale*, 2012, **4**, 4038-4053.
- 68 P. K. Jain, *Struct. Chem.*, 2005, **16**, 421-426.
- 69 M. Manninen, J. Mansikkaaho, H. Nishioka and Y. Takahashi, *Z. Phys. D: At. Mol. Clusters*, 1994, **31**, 259-267.
- 70 J. A. Alonso, *Structure and Properties of Atomic Nanoclusters*, Imperial College Pr, 2005.
- 71 H. Groenbeck and A. Rosen, *Z. Phys. D: At. Mol. Clusters*, 1996, **36**, 153-157.
- 72 L. Han Myoung, G. Maofa, B. R. Sahu, P. Tarakeshwar and K. S. Kim, *J. Phys. Chem. B*, 2003, **107**, 9994-10005.
- 73 P. Jaque and A. Toro-Labbe, *J. Chem. Phys.*, 2002, **117**, 3208-3218.
- 74 E. M. Fernandez, J. M. Soler, I. L. Garzon and L. C. Balbas, *Phys. Rev. B*, 2004, **70**, 165403.
- 75 M. Yang, K. A. Jackson and J. Jellinek, *J. Chem. Phys.*, 2006, **125**, 144308.
- 76 G. H. Guvelioglu, P. P. Ma, X. Y. He, R. C. Forrey and H. S. Cheng, *Phys. Rev. Lett.*, 2005, **94**, 026103.
- 77 K. J. Taylor, C. L. Pettiettehall, O. Cheshnovsky and R. E. Smalley, *J. Chem. Phys.*, 1992, **96**, 3319-3329.
- 78 T. Mineva, N. Russo and M. Toscano, *Int. J. Quantum Chem.*, 2000, **80**, 105-109.
- 79 K. R. S. Chandrakumar, T. K. Ghanty and S. K. Ghosh, *J. Phys. Chem. A*, 2004, **108**, 6661-6666.
- 80 P. Fantucci, V. Bonacickoutecky and J. Koutecky, *Z. Phys. D: At. Mol. Clusters*, 1989, **12**, 307-314.
- 81 E. Janssens, H. Tanaka, S. Neukermans, R. E. Silverans and P. Lievens, *New J. Phys.*, 2003, **5**, 46.1-46.10.
- 82 E. Janssens, S. Neukermans and P. Lievens, *Curr. Opin. Solid State Mater. Sci.*, 2004, **8**, 185-193.
- 83 S. M. Lang, T. M. Bernhardt, R. N. Barnett, B. Yoon and U. Landman, *J. Am. Chem. Soc.*, 2009, **131**, 8939-8951.
- 84 N. Shao, W. Huang, W. N. Mei, L. S. Wang, Q. Wu and X. C. Zeng, *J. Phys. Chem. C*, 2014, **118**, 6887-6892.
- 85 Z. W. Chen, J. M. Yan, W. T. Zheng and Q. Jiang, *Sci. Rep.*, 2015, **5**, 11230.
- 86 W. Zhang, R. Cui, H. Wu and J. Zhu, D. Cheng, *Appl. Surf. Sci.*, 2015, **356**, 282-288.
- 87 X. An, L. Guo and A. Li, *J. Cluster Sci.*, 2015, **26**, 505-527.
- 88 L. Guo and X. Zhang, *J. Phys. Chem. C*, 2014, **118**, 533-543.
- 89 S. Lin and Y. Pei, *J. Phys. Chem. C*, 2014, **118**, 20346-20356.
- 90 S. S. Lee, C. Y. Fan, T. P. Wu and S. L. Anderson, *J. Am. Chem. Soc.*, 2004, **126**, 5682-5683.
- 91 Y. Watanabe, X. Wu, H. Hirata and N. Isomura, *Catal. Sci. Technol.*, 2011, **1**, 1490-1495.
- 92 W. E. Kaden, T. Wu, W. A. Kunkel and S. L. Anderson, *Science*, 2009, **326**, 826-829.
- 93 Y. Watanabe, *Sci. Technol. Adv. Mater.*, 2014, **15**, 063501.
- 94 T. Imaoka, H. Kitazawa, W. J. Chun and K. Yamamoto, *Angew. Chem. Int. Ed.*, 2015, **54**, 9809-9815.
- 95 T. Imaoka, H. Kitazawa, W. J. Chun, S. Omura, Ken Albrecht and K. Yamamoto, *J. Am. Chem. Soc.*, 2013, **135**, 13089-13095.
- 96 K. Yamamoto, T. Imaoka, W. J. Chun, O. Enoki, H. Katoh, M. Takenaga and A. Sono, *Nat. Chem.*, 2009, **1**, 397-402.
- 97 K. Yamamoto and T. Imaoka, *Acc. Chem. Res.*, 2014, **47**, 1127-1136.
- 98 T. Yoskamtorn, S. Yamazoe, R. Takahata, J. Nishigaki, A. Thivasasith, J. Limtrakul and T. Tsukuda, *ACS Catal.*, 2014, **4**, 3696-3700.
- 99 Z. Wu, M. A. MacDonald, J. Chen, P. Zhang and R. Jin, *J. Am. Chem. Soc.*, 2011, **133**, 9670-9673.
- 100 T. Tsukuda, *Bull. Chem. Soc. Jpn.*, 2012, **85**, 151-168.
- 101 Y. Negishi, T. Nakazaki, S. Malola, S. Takano, Y. Niihori, W.

- Kurashige, S. Yamazoe, T. Tsukuda and H. Häkkinen, *J. Am. Chem. Soc.*, 2015, **137**, 1206-1212.
- 102 M. Zacharska, A. L. Chuvilin, V. V. Kriventsov, S. Beloshapkin, M. Estrada, A. Simakov and D. A. Bulushev, *Catal. Sci. Technol.*, 2016, **6**, 6853-6860.
- 103 J. Mielby, A. J. Kunov-Kruse and S. Kegnæs, *J. Catal.*, 2017, **345**, 149-156.
- 104 G. Kresse and J. Furthmuller, *Comput. Mater. Sci.*, 1996, **6**, 15-50.
- 105 G. Kresse and J. Furthmuller, *Phys. Rev. B*, 1996, **54**, 11169-11186.
- 106 G. Kresse and D. Joubert, *Phys. Rev. B*, 1999, **59**, 1758-1775.
- 107 P. E. Blochl, *Phys. Rev. B*, 1994, **50**, 16223-16233.
- 108 J. P. Perdew and Y. Wang, *Phys. Rev. B*, 1992, **45**, 17953-17979.
- 109 J. Klimes, D. R. Bowler and A. Michaelides, *J. Phys.: Condens. Matter*, 2010, **22**, 022201.
- 110 J. Klimes, D. R. Bowler and A. Michaelides, *Phys. Rev. B*, 2011, **83**, 195131-.
- 111 S. Nose, *J. Chem. Phys.*, 1984, **81**, 511-519.
- 112 G. Henkelman, B. P. Uberuaga and H. Jonsson, *J. Chem. Phys.*, 2000, **113**, 9901-9904.
- 113 L.C. Grabow and M. Mavrikakis, *ACS Catal.*, **2011**, **1**, 365-384.

Table 1 Total Energy difference between adsorbed formate (HCOO) and adsorbed carboxyl (COOH) on Au<sub>n</sub> (n=4-25) clusters.  $dE = E(\text{HCOO}/\text{Au}_n) - E(\text{COOH}/\text{Au}_n)$ . Negative entries indicate more stable adsorbed formate (HCOO) isomer.

	Au <sub>4</sub>	Au <sub>5</sub>	Au <sub>6</sub>	Au <sub>7</sub>	Au <sub>8</sub>	Au <sub>9</sub>	Au <sub>10</sub>	Au <sub>11</sub>	Au <sub>12</sub>	Au <sub>13</sub>	Au <sub>14</sub>	Au(211)
dE(eV)	-0.22	-0.63	0.02	-0.09	-0.02	-0.18	-0.35	-0.16	-0.36	-0.36	-0.25	-0.35
	Au <sub>15</sub>	Au <sub>16</sub>	Au <sub>17</sub>	Au <sub>18</sub>	Au <sub>19</sub>	Au <sub>20</sub>	Au <sub>21</sub>	Au <sub>22</sub>	Au <sub>23</sub>	Au <sub>24</sub>	Au <sub>25</sub>	
dE(eV)	-0.25	-0.39	-0.25	-0.54	-0.45	-0.09	-0.13	-0.27	-0.18	-0.67	-0.36	

Table 2 Calculated activation energy (E<sub>a</sub>) of HCOOH dehydrogenation to HCOO (HCOOH\* + 2\* ⇌ HCOO\*\* + H\*) on Au<sub>n</sub> (n=4-25) clusters. E<sub>a</sub> on Au(211) is given for comparison.

	Au <sub>4</sub>	Au <sub>5</sub>	Au <sub>6</sub>	Au <sub>7</sub>	Au <sub>8</sub>	Au <sub>9</sub>	Au <sub>10</sub>	Au <sub>11</sub>	Au <sub>12</sub>	Au <sub>13</sub>	Au <sub>14</sub>	Au(211)
E <sub>a</sub> (eV)	0.92	0.76	1.47	0.92	1.25	1.01	1.14	1.16	1.00	1.02	1.14	1.20
	Au <sub>15</sub>	Au <sub>16</sub>	Au <sub>17</sub>	Au <sub>18</sub>	Au <sub>19</sub>	Au <sub>20</sub>	Au <sub>21</sub>	Au <sub>22</sub>	Au <sub>23</sub>	Au <sub>24</sub>	Au <sub>25</sub>	
E <sub>a</sub> (eV)	1.14	1.09	0.84	0.67	0.85	1.35	1.14	1.17	1.20	0.86	0.93	

Table 3 Activation energy (Ea) and reaction energy ( $\Delta E$ ) of key elementary steps in HCOOH decomposition on several Au<sub>n</sub> clusters. All values are relative to the best initial/final states and are reported in eV.

Elementary reactions	Au <sub>4</sub>		Au <sub>5</sub>		Au <sub>7</sub>		Au <sub>17</sub>		Au <sub>18</sub>		Au <sub>19</sub>		Au(211) <sup>a</sup>	
	Ea	$\Delta E$	Ea	$\Delta E$	Ea	$\Delta E$	Ea	$\Delta E$	Ea	$\Delta E$	Ea	$\Delta E$	Ea	$\Delta E$
1 HCOOH(g) + * → HCOOH*		-1.02		-0.58		-0.65		-0.50		-0.54		-0.42		-0.28
2 HCOOH* + 2* → HCOO** + H*	0.92	-0.50	0.76	-0.16	0.92	-0.08	0.84	-0.12	0.67	-0.18	0.85	0.15	1.20	0.40
3 HCOO** → CO <sub>2</sub> (g) + H* + *	1.09	0.15	1.44	0.27	0.93	-0.44	1.15	-0.03	1.04	0.27	1.07	0.22	1.03	0.04
4 2H* → H <sub>2</sub> * + 2*	0.26	0.17	0.49	0.28	0.74	0.48	0.83	0.41	0.87	0.66	0.50	0.07	0.55	-0.02
5 HCOOH* + * → COOH* + H*	--	--	1.06	0.13	1.15	0.27	--	--	1.22	0.33	1.36	0.59	1.37	0.80
6 COOH* → CO <sub>2</sub> (g) + H*	--	--	0.98	-0.36	1.04	-0.53	--	--	1.19	-0.27	1.10	-0.22	0.96	-0.31
7 COOH* + * → CO* + OH*	--	--	0.35	-2.78	0.84	-3.00	--	--	0.53	-2.61	0.56	-3.22	1.10	0.58
8 OH* + H* → H <sub>2</sub> O* + *	--	--	1.19	-0.41	0.86	-0.32	--	--	0.80	-0.60	0.63	-0.71	0.69	-0.92
9 CO* → CO(g) + *		1.74		1.27		1.24		1.15		1.11		0.87		0.73
10 H <sub>2</sub> O* → H <sub>2</sub> O(g) + *		--		0.41		0.44		--		0.39		0.32		0.25
11 H <sub>2</sub> * → H <sub>2</sub> (g) + *		0.70		0.29		0.30		0.12		0.19		0.05		--

<sup>a</sup>Ea and  $\Delta E$  values on Au(211) are relative to the infinite separation of species in the initial/final states.

Table 4 Interaction energy between H and HCOO, H and H in their best co-adsorbed states on several promising Au<sub>n</sub> clusters. Negative values indicate attractive interaction; positive values repulsive interaction.

Interaction energy (eV)	Au <sub>4</sub>	Au <sub>5</sub>	Au <sub>7</sub>	Au <sub>17</sub>	Au <sub>18</sub>	Au <sub>19</sub>
H+HCOO	-1.17	1.33	0.81	0.18	-0.23	0.69
H+H	-0.64	1.34	1.29	0.44	-0.31	0.81

Table 5 Adjustments needed in DFT derived BE ( $\Delta$ BE) of the intermediates and transition state energy ( $\Delta$ ETS) of the elementary steps on Au<sub>4</sub>, Au<sub>5</sub>, Au<sub>7</sub> and Au<sub>17</sub>-Au<sub>19</sub> corresponding to the best fit and the corresponding model predicted surface coverage  $\theta$ .

Adjustments (eV)	Au <sub>4</sub>	Au <sub>5</sub>	Au <sub>7</sub>	Au <sub>17</sub>	Au <sub>18</sub>	Au <sub>19</sub>	Au(211)
$\Delta$ BE(HCOOH)	0.10		0.57				
$\Delta$ BE(HCOO)	-0.15		-0.02	-0.09	-0.10	-0.10	0.10
$\Delta$ BE(H)	0.41	0.62	0.81	0.22		0.32	0.08
$\Delta$ ETS(HCOOH $\rightarrow$ HCOO+H)		-0.15	-0.28	-0.36	-0.16	-0.33	-0.65
$\Delta$ ETS(HCOO $\rightarrow$ CO <sub>2</sub> +H)	-0.51	-0.32		-0.41	-0.29	-0.21	-0.45
$\Delta$ ETS(H+H $\rightarrow$ H <sub>2</sub> )		-0.21		-0.21	-0.05	-0.43	
Surface coverage (ML)	Au <sub>4</sub>	Au <sub>5</sub>	Au <sub>7</sub>	Au <sub>17</sub>	Au <sub>18</sub>	Au <sub>19</sub>	Au(211)
$\theta$ (H)	0.00	<0.01	<0.01	<0.01	0.00	<0.01	0
$\theta$ (HCOO)	0.00	0.10-0.58	0.11-0.50	0.06-0.34	0-0.10	0.10-0.50	0
$\theta$ (HCOOH)	0.04-0.40	0.00	0.00	0.00	0.00	0.00	<0.05



Atomic scale size-sensitivity of the catalytic properties of sub-nanometer gold clusters for HCOOH decomposition.